A&A 401, 339–346 (2003)
DOI: 10.1051/0004-6361:20021769

Astronomy & Astrophysics

Microlensing of circumstellar envelopes

II. Emission lines from radial and azimuthal flow during fold caustic crossings

H. M. Bryce[1,2], R. Ignace[2], and M. A. Hendry[1]

[1] Dept. of Physics & Astronomy, University of Glasgow, Glasgow G12 8QQ, UK
[2] Dept. of Astronomy, University of Wisconsin, 475 North Charter Street, Madison, Wisconsin, 53706, USA

Received 17 October 2002 / Accepted 2 December 2002

Abstract. This paper examines the line profile evolution due to bulk motion in circumstellar envelopes during microlensing fold caustic crossing events. These events have recently been shown to be a sensitive probe of stellar surface brightness profiles, thus providing a means – through both photometric and spectroscopic observations – to constrain and test stellar atmosphere models. Here it is demonstrated, through the examination of simplified line profiles, that spectroscopic studies of fold caustic crossings could also prove to be a powerful diagnostic of bulk motion in circumstellar envelopes.

Key words. gravitational lensing – stars: circumstellar matter

1. Introduction

As suggested by Paczyński (1986), gravitational microlensing has proved to be an effective tool for examining the distribution and nature of dark matter in the Milky Way, with more than a thousand candidate events now identified.

In the typical microlensing situation of a point source lensed by a point lens, the (time-dependent) amplification is given by

$$A(t) = \frac{u^2+2}{u\sqrt{u^2+4}}, \tag{1}$$

where the projected lens-source separation, u, is

$$u(t) = \sqrt{u_0^2 + \frac{(t-t_0)^2}{t_{\rm E}^2}}, \tag{2}$$

where t_0 is the time of maximum amplification, which occurs at $u = u_0$, the minimum impact parameter, and $t_{\rm E}$ is the characteristic timescale of the event. Both u and u_0 are expressed in units of the angular Einstein ring radius, which is defined as

$$\theta_{\rm E} = \sqrt{\frac{4GM}{c^2}\frac{(D_{\rm S}-D_{\rm L})}{D_{\rm S}D_{\rm L}}}, \tag{3}$$

where M, $D_{\rm S}$, $D_{\rm L}$ are the lens mass, source distance and lens distance respectively. The timescale $t_{\rm E}$ may be written as

$$t_{\rm E} = \frac{\theta_{\rm E}}{\mu_{\rm rel}}, \tag{4}$$

where $\mu_{\rm rel}$ is the relative proper motion of the lens. Thus for a standard point lens, point source event, the light curve shape displays a degeneracy among the lens parameters, in that one cannot separately determine $\theta_{\rm E}$ and $\mu_{\rm rel}$. Consequently, one cannot separately constrain the mass and location of the lens, as to do so one would require additional information such as the transverse velocity from annual parallax devations (Gould 1992).

However, a number of authors (see e.g. Nemiroff & Wickramasinghe 1994; Witt & Mao 1995; Witt 1995; Simmons et al. 1995; Peng 1997) have pointed out that a so-called *finite source* treatment is required at small lens-source separations, since the source can no longer be approximated as a point. Such events can break the degeneracy between lens parameters (Gould 1994) as the source size may be determined from the lightcurve, allowing the Einstein radius of the lens to be calculated. This is because the amplification of a finite source is given by an intensity weighted average over the projected surface of the source, and thus is sensitive to the source parameters.

It has been noted by a number of authors that such an opportune event can also be used to probe the astrophysical properties of the source (see Gould 2001 and references therein for a detailed review). The microlensed lightcurve of a limb-darkened star, for example, has been shown to produce a characteristic chromatic signature as the lens can be thought of as "seeing" a star of differing radii at different wavelengths (Valls-Gabaud 1998). Specific astrophysical applications of extended source microlensing considered in recent literature include: the use of photometric, spectroscopic and

Send offprint requests to: H. M. Bryce,
e-mail: bryce@astro.wisc.edu

polarimetric observations to constrain stellar atmosphere models (Simmons et al. 1995; Simmons et al. 1995; Newsam et al. 1998; Heyrovský et al. 2000; Bryce et al. 2002), detection of starspots (Heyrovsky & Sasselov 2000; Hendry et al. 2002), and probing circumstellar envelopes (Ignace & Hendry 1999, hereafter IH99).

In IH99 the authors considered the evolution in line profile shape of a geometrically and optically thin shell of circumstellar material in uniform expansion or rotation, lensed by a point mass lens. In the absence of lensing, both of these velocity field models would produce "flat top" line profiles, and would therefore be indistinguishable, since they are geometrically degenerate when one integrates over the unresolved volume of the circumstellar envelope. The effect of lensing, however, was shown to break this degeneracy. In particular for an expanding shell, the amplification of the line profile was *symmetric* about line centre throughout the lensing event, while for a rotating shell the evolution of the line profile shape was distinctly *asymmetric*. Thus microlensing was seen to yield useful information about the velocity field in the extended envelope. IH99 also described the impact of microlensing in less idealised cases, including the use of multiline observations to infer the ionisation stratification of circumstellar envelopes and the use of polarisation observations to constrain the properties of "clumpy" winds.

The principal limitation of the results of IH99, however, was that only point mass lensing events were considered. The discriminatory power of line profile shapes was shown to be significant, but only for the case of transit events (i.e., events with an impact parameter smaller than the source radii). Following Valls-Gabaud (1998), IH99 estimated the fraction of candidate microlensing events which are transits to be about 5%, which is higher than the number of confirmed transit events which have been observed to date – namely the event MACHO 95–30. Given the considerable additional effort required to carry out spectroscopic observations, it is clearly not practical at present to monitor spectroscopically large fields of stars in the hope of fortuitously "catching" the point lens transit of an extended circumstellar envelope – whatever the useful astrophysical potential of such data. Fortunately, however, an alternative and more practicable observational strategy now exists.

The other major area of recent interest in non-standard microlensing events is the study of complex lens systems – as produced by, for example, a star with a low mass stellar or planetary companion. In such cases the amplification function takes a non-analytical form and caustic structures are produced in the lens plane. These are regions of formally infinite amplification; however in practice, the amplification remains finite because the background star must be treated as a finite source. Although such events contribute only a small fraction (∼5%) to the total number of predicted events, the lightcurves from binary lenses have been extensively studied (see e.g. Mao & Paczynski 1991; Mao & Di Stefano 1995; Dominik 1998). These lightcurves will show a large rise in magnification if the source crosses into a caustic structure (which can generally be treated as a straight line, or *fold caustic*, since any curvature in the caustic is likely to be on a much larger scale than the angular radius of the source). An anomaly "alert" can then be triggered by the dramatic rise in amplification, allowing extensive monitoring of the system to be carried out during the second crossing as the source exits the closed caustic contour.

It is the possibility of "alert" responses to fold caustic crossings which now makes the spectroscopic monitoring of microlensing events an observationally realistic prospect, and a strategy which has recently been carried out successfully for the spectacular EROS BLG–2000–05 event (Albrow et al. 2001; Castro et al. 2001). The number of caustic crossing events is modest but significant; 12 crossings out of 221 events in the OGLE II survey (Jaroszynki 2002) and 14 crossings out of 350 events from the MACHO database (Alcock et al. 2000). Thus, it is now timely to repeat the calculations of IH99 for the case of a fold caustic crossing.

The structure of this paper is as follows. In Sect. 2, following IH99, we derive the unlensed line profile for geometrically and optically thin shells that are either rotating or expanding. In Sect. 3 we consider the time evolution of the line profile shape when such shells undergo a high amplification fold caustic crossing, and consider the diagnostic power of microlensing in this case. Finally, in Sect. 4 we discuss the observational implications of our results.

2. Expanding and rotating shells in circumstellar envelopes

As in IH99 we consider only the highly simplified case of a geometrically and optically thin spherical shell in either uniform expansion or uniform rotation. Furthermore, for our calculation of the unlensed emission line profile the source itself is approximated as a point source of illumination, allowing the effects of absorption and occultation to be ignored. The consequence of these assumptions is that every photon escapes from the envelope and so volume integrals over the envelope can be computed to determine the line profile.

For an envelope in bulk motion, where the flow speed greatly exceeds the thermal broadening, the locus of points contributing to the emission at any particular frequency is confined to an "isovelocity zone". These zones are described by the Doppler shift formula,

$$\nu_Z = \nu_0 \left(1 - \frac{\upsilon_Z}{c}\right). \tag{5}$$

For observer coordinates (X, Y, Z) with the line of sight along Z, ν_Z is the Doppler shifted frequency and υ_Z represents the projection of the flow speed onto the line of sight, $\upsilon_Z = -\boldsymbol{\upsilon}(\boldsymbol{r}) \cdot \hat{\boldsymbol{z}}$, where $\hat{\boldsymbol{z}}$ is a unit vector along the line-of-sight. It is by consideration of the geometry of the isovelocity zones produced by differing bulk motions, in this case rotating versus expanding flows, that microlensing can be shown to be a powerful probe of circumstellar envelopes.

For constant expansion with $\boldsymbol{\upsilon} = \upsilon_0 \hat{\boldsymbol{r}}$, where $\hat{\boldsymbol{r}}$ is the unit vector along the radial direction to (X, Y, Z), the velocity shift along the line-of-sight becomes $\upsilon_Z = -\upsilon_0 \cos\theta$, where θ is the angle between $\hat{\boldsymbol{r}}$ and $\hat{\boldsymbol{z}}$. For a constant υ_Z (i.e., for a particular isovelocity zone), the angle θ must also be constant. This situation is illustrated in Fig. 1, where an isovelocity zone is

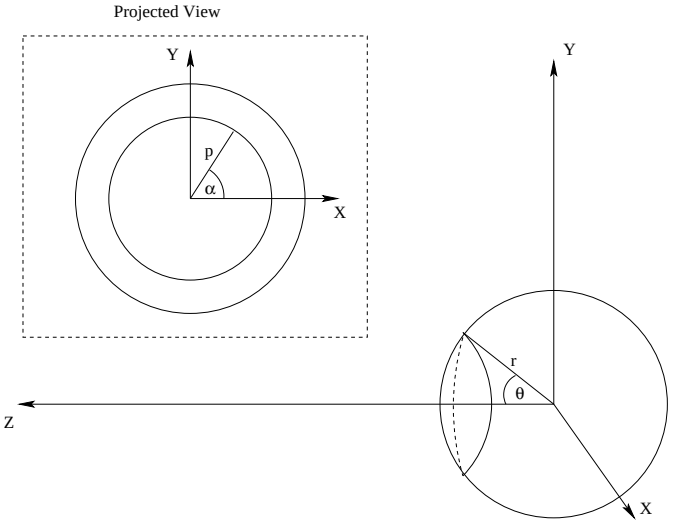

Fig. 1. The geometry of uniformly expanding shells. The lower diagram shows the 3-dimensional view with the observer's line-of-sight coincident with the Z-axis. The circular ring centred on the Z-axis represents an isovelocity zone characterised by Doppler shift υ_Z. The upper box shows the same isovelocity zone, defined by circular polar coordinates p and α, in projection.

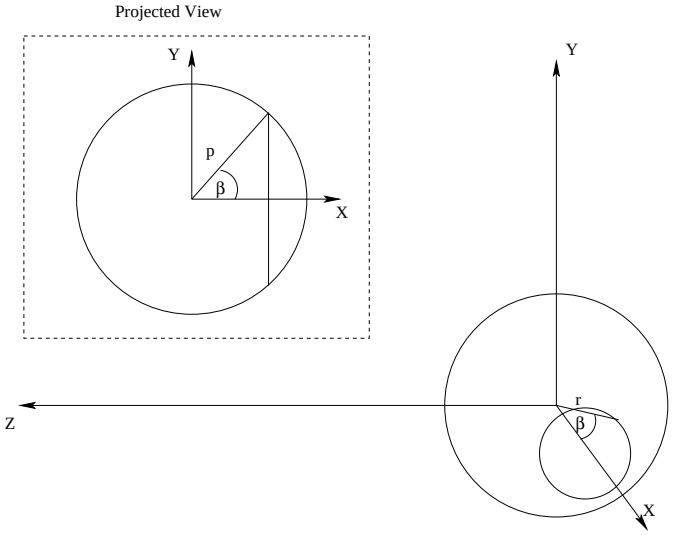

Fig. 2. The geometry of uniformly rotating shells shown in the same manner as Fig. 1. The isovelocity zone is now a circular ring centred on the X-axis with opening angle β, seen in projection as a strip in the upper box.

shown as a ring centred on the Z-axis. For line intensity $I_\nu(p)$ with p the cylindrical radius at the source plane, the flux of line emission from this ring is given by

$$F_\nu = 2\pi I_\nu(p) p \, \mathrm{d}p. \tag{6}$$

This observed flux can also be written, with $j_\nu(r)$ the emissivity, as

$$F_\nu = \int_{\upsilon_z} j_\nu(r) \, \mathrm{d}V \tag{7}$$

i.e., a volume integral over the isovelocity zone, as expected for an optically thin line. Performing the integral yields the expression

$$F_\nu = \frac{2\pi r^2 j_\nu(r)}{\upsilon_0} \mathrm{d}r \, \mathrm{d}\upsilon_Z. \tag{8}$$

As the velocity shift term υ_Z does not appear here, F_ν is constant with frequency, or *flat topped*.

To consider the case of a uniformly rotating shell, it is convenient to introduce spherical polar coordinates, (r, ϑ, φ) centred on the source. The rotation velocity in this case is given by $\boldsymbol{v} = \upsilon_0 \hat{\boldsymbol{\varphi}}$ where $\hat{\boldsymbol{\varphi}}$ is the unit vector in the direction of increasing φ. The velocity shift along the observer's line-of-sight is $\upsilon_Z = -\upsilon_0 \sin\vartheta \cos\varphi \sin i$, where i is the inclination of the rotation axis to the observer's line-of-sight. Since the inclination is fixed for a given shell, and since it can be shown using spherical trigonometry that $\sin\vartheta \cos\varphi = \cos\beta$, the isovelocity zones once again reduce to circular rings with opening angle β, as shown in Fig. 2. Thus, the profile shape is again flat topped and the flux of line emission from a rotating shell is

$$F_\nu = \frac{2\pi r^2 j_\nu(r)}{\upsilon_0 \sin i} \mathrm{d}r \, \mathrm{d}\upsilon_Z. \tag{9}$$

In summary, both uniformly expanding and rotating shells produce flat-top line profiles, and hence are indistinguishable based on line profile shape (although arguably, rotating shells would tend to have smaller velocities than expanding shells). The geometries of the isovelocity zones that produce emission are clearly different, however: in the expanding case the isovelocity ring is circular in projection, but in the rotating case the ring is viewed edge on and so appears as a strip. In the expanding case the shells are front-back symmetric – i.e., every isovelocity zone on the front side is identical to one on the back, but with opposite υ_Z sign, whereas in the rotating case the shells are left-right anti–symmetric.

3. The effects of high amplification microlensing events

For an extended source, the amplification due to microlensing by a point mass lens is given by the intensity weighted amplification averaged over the surface of the source, i.e.

$$A_{\mathrm{ext}} = \frac{\int_0^{2\pi} \int_0^{s_*} I(s,\alpha) A(u) s \, \mathrm{d}s \mathrm{d}\alpha}{\int_0^{2\pi} \int_0^{s_*} I(s,\alpha) s \, \mathrm{d}s \, \mathrm{d}\alpha} \tag{10}$$

where (s, α) are the angular coordinates at the source plane, s_* is the angular radius of the source, which is normalised to the (angular) Einstein radius of the lens and the amplification function $A(u)$ is as given in Eq. (1) for a point mass lens and the projected lens source separation $u = u(s, \alpha, t)$.

In IH99, the microlensing lightcurves produced by circumstellar envelopes with uniform expansion and rotation were examined using the above treatment for a variety of event parameters. It was shown that only transit events would provide the means to discriminate between the source models. In this work, fold caustic crossings are considered, and as the amplification is formally infinite for such an event, each crossing requires

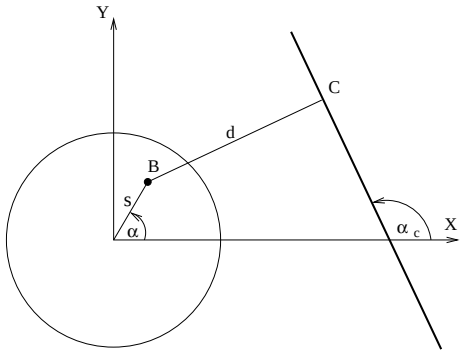

Fig. 3. The geometry associated with a fold caustic crossing, with the coordinates centred on the source.

an extended source treatment to be accurately modelled. The question then remains: does the geometry of such an event allow the degeneracy between rotating and expanding shells to be broken?

Naturally, we are only concerned with the crossing itself rather than the lightcurve as a whole, as we require a high level of differential amplification across the source if we wish to examine the source. This allows us to consider only the region of the lightcurve in which the inverse square root approximation adequately serves to model the excess amplification, due to the production of extra images within the caustic structure (Schneider et al. 1992), here we consider d as the projected source caustic separation (i.e., the perpendicular distance between the source and the caustic):

$$A(d) = \begin{cases} A_0 + \frac{b_0}{\sqrt{d}} & (d > 0), \\ A_0 & (d < 0), \end{cases} \tag{11}$$

where A_0 is the total magnification of the 3 non-caustic images and $b_0 = 1$ for typical caustics. Furthermore this approximation assumes that the crossing does not occur in the vicinity of a cusp and that the curvature of the caustic is small in comparison with the source size.

The geometry of such a situation in illustrated in Fig. 3. Here B denotes a position on the source disk at $(x, y) = (s\cos\alpha, s\sin\alpha)$, separated by a perpendicular distance d from point C on the caustic. The amplification from this surface element (when within the caustic) is $A_0 + 1/\sqrt{d}$. We employ a coordinate system centred on the source rather than the caustic (as is more natural to do in this case, as the source is the object under study), so at time t the caustic is separated by X_c along the X-axis from the centre of the source. The caustic itself is inclined to the X-axis at an angle α_c. In the following series of examples, we consider the caustic progressing uniformly along the X-axis. Moreover, where relevant, we consider the axis of rotation to be coincident with the Y-axis, i.e., with $i = 90°$.

Figures 4, 5 and 6 present sequences of line profiles for both expanding and rotating shells. Results are plotted as the ratio of the lensed flux to the unlensed flux (the latter being just the flat-top profile), plus a constant offset introduced between each timestep to display better the time evolution of the profile shape. The sequence begins when the centre of the source is 3 source radii inside the caustic structure, in the lowest line profile shown. The central line profile in each figure corresponds to the caustic crossing the centre of the source, and the uppermost line profile corresponds to the centre of the source lying 3 source radii outside the caustic structure. The source size in these figures is taken to be $s_* = 0.1$. This value is comparable to – albeit slightly larger than – the estimated stellar radius for MACHO–95–30 (Alcock et al. 1997) and is also the value adopted in Hendry et al. (2002), in the context of microlensing stellar photospheres. While it was argued in Hendry et al. that there could be some merit in considering smaller sources, in fact, a source radius of $0.1\theta_E$ is more justified in this paper since we are considering here envelopes of circumstellar material, which are more extended than the photosphere. In any event, it is worth noting that altering the source size changes the overall level of amplification of the line profile (with a smaller source producing a higher amplification as expected) but does not affect the profile velocity of the peak amplification at each timestep. In other words a rescaling of only the vertical axis would be required to recover an identical line profile shape, for differing source radii.

Figure 4 shows the line profile evolution for rotating and expanding shells in the case of $\alpha_c = 90°$. Note, that the line profile of the rotating shell admits an analytic solution for a general angle α_c, which we derive the Appendix. In both the expanding and rotating cases, we see that the line profiles remain essentially flat-topped until the fold caustic begins to cross the source (which occurs on the ninth timestep, about one third of the way from the bottom of the figure). At this point one immediately sees that there is a clear difference in the line profile evolution between the two models.

The rotating case exhibits a series of highly asymmetric spikes – both in shape and velocity – which migrate across the line profile as the event progresses until the transit phase ends, at which point the profile quickly returns to a flat-top. In the expanding case, when the transit begins we see at first a single spike feature, which later evolves into a double spiked feature, symmetric about line centre. These spikes migrate outwards and then into a broad "top hat" feature in the profile (see e.g., the fifteenth and sixteenth timesteps). Thereafter, the profile again returns to the unamplified flat-top.

It is straightforward to understand the origin of the features described above. Consider first the rotating case and recall that here the isovelocity zones appear as strips perpendicular to the X-axis. Since the amplification at any instant is dominated by the portion of the circumstellar envelope being transited by the caustic, the migration of the spike feature across the line profile results from the caustic effectively lensing in turn a series of different isovelocity zones. Moreover, the asymmetric shape of each spike is a consequence of the asymmetry of our amplification function with respect to the fold caustic – i.e. only those isovelocity zones inside the caustic structure are producing excess amplification.

In contrast, in the expanding shell case – where the isovelocity zones are front-back symmetric – at any instant during the crossing the amplification will be dominated by two sources of flux: one from the "front" of the envelope and one with equal but opposite sign velocity shift from the "back" of the envelope. This produces an amplified line profile which is still symmetric about line centre. As the fold caustic begins to transit the source

(which of course means that part of the source begins to *exit* the caustic structure, and thus no longer produces excess amplification) the line profile begins to evolve. The spike feature seen at first occurs because the amplification is dominated by a very small range of isovelocity zones. The peak then splits into resolved "front" and "back" components, and migrates out to the wings as the event proceeds. This is because the amplification is being dominated by regions closer to the centre of the source, where the isovelocity zones of greatest radial velocity are situated. The central line profile shows peaks in the wings as (essentially *all* of) the isovelocity zones corresponding to the peak amplification are very close to the caustic. Conversely, in the centre of the line profile – corresponding to isovelocity rings close to the *limb* of the source – there is much less amplification because a much smaller fraction of the rings are then close to the caustic. After the caustic has crossed the centre of the source we continue to see this effect, but now it is isovelocity zones of progressively smaller radial velocity which are preferentially amplified. This results in the migration of the peaks back towards the centre of line profile and the peaks begin to level off. Moreover, in the final timesteps during the transit, we see a "top hat" type line profile. The "brim" of the top hat is not amplified as the isovelocity zones that would contribute to those portions of the line profile are now completely outside the caustic.

It is important to note that the rotating shells experience higher levels of amplification than the expanding shells at any given instant during the event, because in the rotating case virtually all of an individual isovelocity zone is crossing the caustic. The effect of this is clear in the difference between the vertical axis scale in the left and right panels of Fig. 4.

The effects of changing the inclination of the caustic can be seen in Figs. 5 and 6, which show the line profile evolution for $\alpha_c = 100°$ and $\alpha_c = 120°$ respectively. There are several interesting features apparent in these figures. In particular, we see that the rotating line profiles are somewhat "smeared out" compared with those of Fig. 4. This is because at any instant the number of isovelocity zones being crossed by the caustic is now slightly larger. Note also that rotating the position angle of the source rotation axis in the plane of the sky would result in precisely the same effect on the line profiles as rotating the angle of the caustic with respect to the X-axis.

In the case of the expanding line profiles we can see that the effects of the amplification begin slightly earlier in the sequence of line profiles. This is not surprising, since the inclination of the fold caustic means that, at early timesteps, the source lies closer to the caustic – or equivalently the caustic begins to transit the source (albeit obliquely) at an earlier time. Note, however, that at first we see only very small changes in the amplified flux, since only a relatively small fraction of the outer part of the source (or equivalently the central part of the line profile) experiences this "early" transit of the caustic. Note also that, due to the radial symmetry of the isovelocity zones, at any timestep the expanding line profile for an inclined caustic is identical to the line profile for a caustic normal to the X-axis, but with a re-scaled impact parameter. In contrast, there is no such trivial re-scaling for the rotational case, since changing the inclination of the caustic also changes the number of isovelocity zones crossed at each timestep.

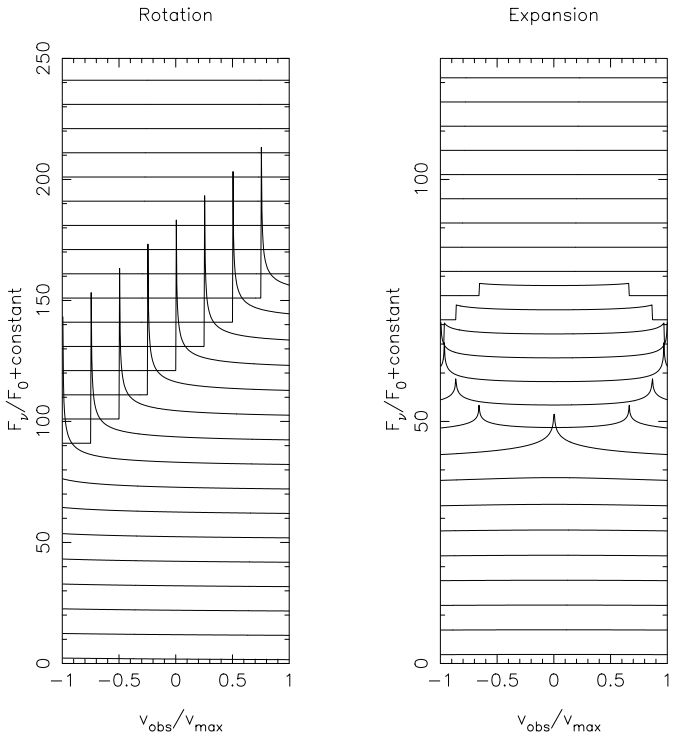

Fig. 4. The line profile (with time increasing upwards) of an uniformly rotating shell (left panel) and an uniformly expanding shell (right panel) for an event trajectory with $\alpha_c = 90°$.

4. Discussion

In this work we have studied the behaviour of emission line profiles from optically thin envelopes in either uniform expansion or uniform rotation. It has been shown that the differential amplification of the source provided by a fold caustic crossing is sufficient to break the degeneracy between the unlensed line profiles for the two cases considered. Furthermore we have shown that this result is valid for differing event trajectories, so that microlensing is a robust technique for diagnosing bulk flow. We should also reiterate that the fold caustics studied here would provide much better observational prospects than the point mass lenses considered in IH99, as the event alert created by the first caustic crossing creates the opportunity for intensive photometric and spectroscopic monitoring.

Note that the significant difference between the microlensed line profiles for rotating and expanding shells is also robust to changes in the shape of the caustic. Following the approach of Fluke & Webster (1999) we have approximated the caustic as a parabola, rather than a straight line and repeated our calculations of the evolution of emission line profiles. We find in this case that our rotating and expanding shell models are easily still distinguishable from each other, despite the number of isovelocity zones being crossed at any instant increasing, provided that the curvature of the caustic is not so large as to make the overall size of the caustic structure comparable with that of the source. In such a case, however, we could not hope

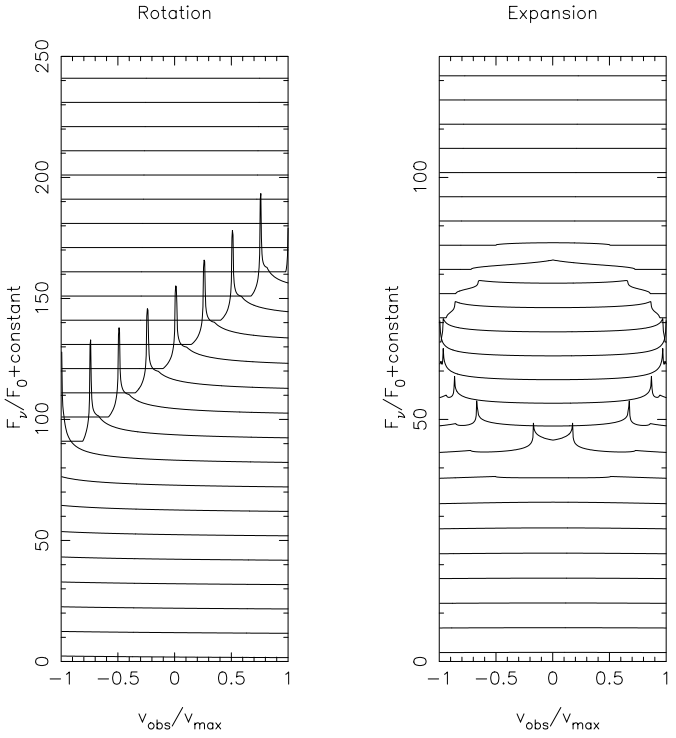

Fig. 5. The line profile (with time increasing upwards) of an uniformly rotating shell (left panel) and an uniformly expanding shell (right panel) for an event trajectory with $\alpha_c = 100°$.

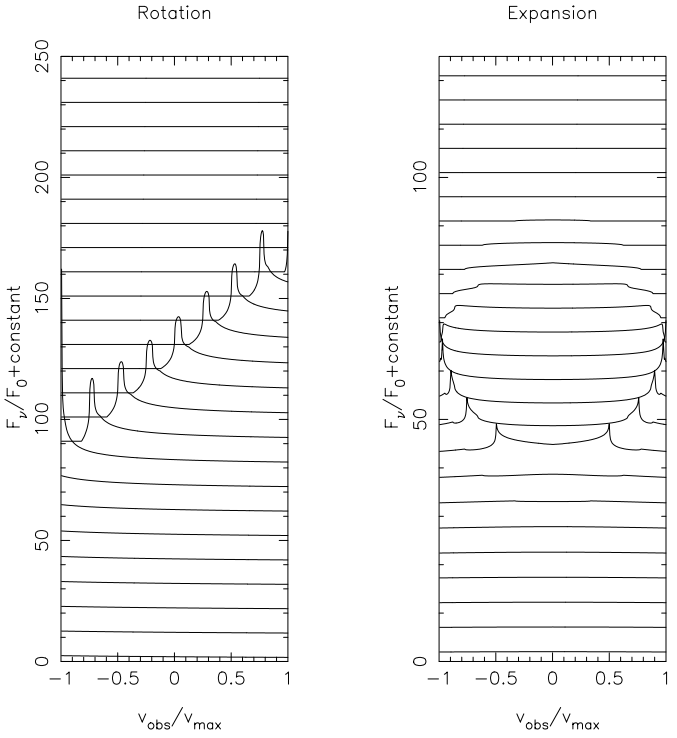

Fig. 6. The line profile (with time increasing upwards) of an uniformly rotating shell (left panel) and an uniformly expanding shell (right panel) for an event trajectory with $\alpha_c = 120°$.

to observe any spectral line evolution using the alert-response technique that motivated this study.

The bulk flow models considered in this work are, of course, simplified, and more realistic envelopes need to be considered. For example in the case of rotation, the amount of lateral motion in a circumstellar envelope will be a function of radius, presumably with small speeds at larger radius. Unless these motions are associated with a Keplerian disk, the extended envelope will rotate at around the stellar rotation speed and less. Consequently, the emission from the envelope may well be superposed with a photospheric absorption profile. Maoz & Gould (1994) and Gould (1997) considered the effects of microlensing for photospheric lines from rotating stars. They chose to focus on line centroid shifts, as opposed to the line profile evolution presented here, partly in anticipation of line broadening by stellar turbulence. Such effects will also influence the lensing of rotating circumstellar envelopes, and a shift of the line centroid will still result. However, in early-type stars, the stellar rotation speeds are around 100–200 km s^{-1}, and similar values are inferred from the emission lines (e.g., Hα) for the rotating disks of Be stars. Unfortunately, these early-type stars are much less likely to be lensed.

The expansion case has somewhat different observational concerns. Wind speeds tend to be on order the escape speed of stars, which are generally larger than the stellar rotation speed by factors of several at least. Thus emission lines that form in these relatively fast moving expanding flows should be resolvable and significantly wider than any photospheric absorption contribution, even if the star is rotating.

Although we did not specifically consider pulsating atmospheres, our analysis in conjunction with the previous work on lensing of rotating stars allows us to discern the salient effects. The case of rotation produces a line asymmetry (equivalently, a variation of the line centroid position) because the projected velocity field is left-right antisymmetric. The expansion case produces a symmetric profile because the projected velocity field is back-front symmetric, but this is only the case if both stellar occultation and absorption of stellar continuum radiation by the intervening wind material are ignored. In the case of uniform radial pulsations, one can liken the influence of microlensing to our results for an expanding spherical shell, except that the effect on the far hemisphere is to be ignored, since that will be occulted. Although for pulsating stars, the effect will occur for a photospheric absorption line, the point is that the line symmetry is lost, and a shift of the line centroid will result. In contrast to stellar rotation, the variation of the centroid shift will depend on the pulsation period relative to the duration of the lens event (i.e., $t_{\rm E}$).

Our analysis could be extended to the optically thick case, for example, and to contrast the impact of microlensing on the evolution of e.g. resonance lines and recombination lines. One could also extend our analysis to more realistic velocity laws, such as linear (homologous) expansion or β velocity laws. There are also possible applications to extragalactic microlensing, e.g. ouflows from AGN. The observations of Chartas et al. (2002), in which the large equivalent width of the $Fe\ K\alpha$ line was attributed to microlensing, also highlight the possible use of microlensing as a probe of line forming regions, through analysis of the line profile evolution of a range of lines at

different temperatures, densities and optical depths. Whilst we do not expect these idealistic examples to be observed, we do believe that we are providing additional motivation for the continuation of spectroscopic observations of caustic crossing events. Having demonstrated in this paper the clear diagnostic potential of spectroscopic studies of fold caustic crossings, we will extend our analysis to some of these interesting (and more realistic) cases in future work.

Acknowledgements. HMB acknowledges a PPARC studentship. HMB and RI acknowledge support for this research from a NSF grant (AST-9986915)

Appendix A: Analytical solution for rotating shells

Consider a fold caustic which intersects the X-axis at X_c, inclined to the X-axis at an angle α_c as shown in Fig. A.1, where the outside of the caustic structure lies to the right of the caustic. The equation of the caustic is $Y = \tan\alpha_c(X - X_c)$, unless $\alpha_c = \pi/2$ in which case it is $X - X_c$. For the rotating case the isovelocity zones are rings with opening angle β, where $\cos\beta = -v_Z/v_{\max} \equiv -w$; these are seen in projection as lines in the X-Y plane with equation $X = -s_* w$, where s_* is the angular radius of the source, normalised to the angular Einstein radius. The isovelocity zone extends from $Y = -s_*\sqrt{1-w^2}$ to $Y = s_*\sqrt{1-w^2}$ on this line.

Consider first the case where $\alpha_c = \pi/2$. This case is particularly straightforward since the isovelocity zones are all parallel to the caustic. Integrating along each isovelocity zone, and using the fact that in the absence of lensing the line profile is flat-topped, it follows that

$$\frac{F_\nu}{F_0} = \begin{cases} A_0 & (d \le 0), \\ A_0 + \frac{1}{\sqrt{d}} & (d > 0), \end{cases} \tag{A.1}$$

where the perpendicular distance between the isovelocity zone and the caustic is $d = X_c + s_* w$.

For a general angle, α_c, the caustic intercepts the line on which the isovelocity zone lies at Y coordinate $Y_I = -\tan\alpha_c(s_* w + X_c)$. We see that there are three distinct cases to consider:

1. $Y_I \le -s_*\sqrt{1-w^2}$, for which the isovelocity zone lies completely inside the caustic;
2. $Y_I \ge s_*\sqrt{1-w^2}$, for which the isovelocity zone lies completely outside the caustic;
3. $-s_*\sqrt{1-w^2} \le Y_I \le s_*\sqrt{1-w^2}$, for which the isovelocity zone lies partially inside the caustic.

Case (2) trivially gives $F_\nu/F_0 = A_0$. Cases (1) and (3) can be combined into a single integral expression

$$\frac{F_\nu}{F_0} = A_0 + \frac{1}{2s_*\sqrt{1-w^2}} \int_{Y_M}^{s_*\sqrt{1-w^2}} \frac{dY}{\sqrt{d(Y)}} \tag{A.2}$$

where $Y_M = \max(Y_I, -s_*\sqrt{1-w^2})$, and $d(Y)$ is the perpendicular distance from the caustic to a general point on the isovelocity zone with coordinates $(-s_* w, Y)$. Straightforward trigonometry shows that

$$d(Y) = Y\cos\alpha_c + (X_c + s_* w)\sin\alpha_c \tag{A.3}$$

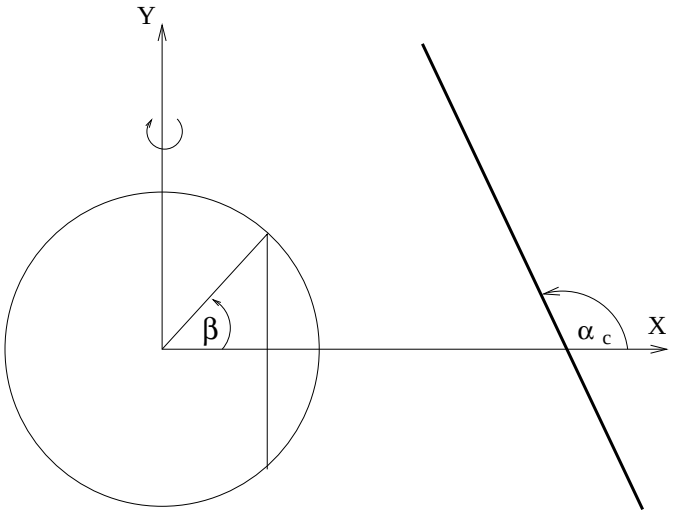

Fig. A.1. The geometry associated with a fold caustic crossing a source with constant rotation.

which then allows the integral in Eq. (A.2) to be solved analytically, yielding the expressions

$$\frac{F_\nu}{F_0} = A_0 + \frac{\sqrt{\Delta_1} - \sqrt{\Delta_2}}{s_*\sqrt{1-w^2}\cos\alpha_c} \tag{A.4}$$

for an isovelocity zone that lies fully inside the caustic, and

$$\frac{F_\nu}{F_0} = A_0 + \frac{\sqrt{\Delta_1}}{s_*\sqrt{1-w^2}\cos\alpha_c} \tag{A.5}$$

for an isovelocity zone that lies partially inside the caustic, where

$$\Delta_1 = (X_c + s_* w)\sin\alpha_c + s_*\sqrt{1-w^2}\cos\alpha_c \tag{A.6}$$

and

$$\Delta_2 = (X_c + s_* w)\sin\alpha_c - s_*\sqrt{1-w^2}\cos\alpha_c. \tag{A.7}$$

References

Albrow, M. D., An, J., Beaulieu, J.-P., et al. 2001, ApJ, 550, L173
Alcock, C., Allen, W. H., Allsman, R. A., et al. 1997, ApJ, 491, 436
Alcock, C., Allsman, R. A., Alves, R. A., et al. 2000, ApJ, 541, 270
Bryce, H. M., Hendry, M. A., & Valls–Gabaud, D. 2002, A&A, 388L, 1
Castro, S., Pogge, R. W., Rich, R., et al. 2001, ApJ, 548, L197
Chartas, G., Agol, E., Eracleous, M., et al. 2002, ApJ, 568, 509
Dominik, M. 1998, A&A, 333, 893
Fluke, C. J., & Webster, R. L. 1999, MNRAS, 302, 68
Gould, A. 1992, ApJ, 392, 442
Gould, A. 1994, ApJ, 421, L71
Gould, A. 1994, ApJ, 483, 98
Gould, A. 2001, PASP, 113, 903
Han, C., Park, S.-H., Kim, H.-I., & Chang, K. 2000, MNRAS, 316, 97
Hendry, M. A., Bryce, H. M., & Valls–Gabaud, D. 2002, MNRAS, 335, 539
Heyrovský, D., & Sasselov, D. 2000, ApJ, 529, 69
Heyrovský, D., Sasselov, D., & Loeb, A. 2000, ApJ, 543, 406
Ignace, R., & Hendry, M. A. 1999, A&A, 341, 201

Jarozynski, M. 2002, Acta Astron., 52, 39
Mao, S., & Di Stefano, R. 1995, ApJ, 440, 22
Mao, S., & Paczyński, B. 1991, ApJ, 374, L37
Maoz, D., & Gould, A. 1994, ApJ, 425, L67
Nemiroff, R. J., & Wickramasinghe, W. 1994, ApJ, 424, 21
Newsam, A. M., Simmons, J. F. L., Hendry, M. A., & Coleman, I. J. 1998, New Astron. Rev., 42, 121
Paczyński, B. 1986, ApJ, 304, 1
Peng, E. W. 1997, ApJ, 475, 43
Schneider, P., Ehlers, J., & Falco, E. E. 1992, Gravitational Lenses (Springer-Verlag)
Simmons, J. F. L., Willis, J. P., & Newsam, A. M. 1995, A&A, 293, L46
Simmons, J. F. L., Newsam, A. M., & Willis, J. P. 1995, MNRAS, 276, 182
Valls-Gabaud, D. 1998, MNRAS, 294, 747
Witt, H. J., & Mao, S. 1994, ApJ, 430, 505
Witt, H. J. 1995, ApJ, 449, 42